Physics Letters A 382 (2018) 1185–1189

Contents lists available at ScienceDirect

Physics Letters A

www.elsevier.com/locate/pla

Dislocation nucleation from symmetric tilt grain boundaries in body-centered cubic vanadium

Shuozhi Xu [a,*], Yanqing Su [b]

[a] California NanoSystems Institute, University of California, Santa Barbara, Santa Barbara, CA 93106-6105, USA
[b] Department of Mechanical Engineering, University of California, Santa Barbara, Santa Barbara, CA 93106-5070, USA

ARTICLE INFO

Article history:
Received 17 December 2017
Received in revised form 9 February 2018
Accepted 2 March 2018
Available online 7 March 2018
Communicated by R. Wu

Keywords:
Molecular dynamics
Vanadium
Dislocation
Grain boundary

ABSTRACT

We perform molecular dynamics (MD) simulations with two interatomic potentials to study dislocation nucleation from six symmetric tilt grain boundaries (GB) using bicrystal models in body-centered cubic vanadium. The influences of the misorientation angle are explored in the context of activated slip systems, critical resolved shear stress (CRSS), and GB energy. It is found that for four GBs, the activated slip systems are not those with the highest Schmid factor, i.e., the Schmid law breaks down. For all misorientation angles, the bicrystal is associated with a lower CRSS than their single crystalline counterparts. Moreover, the GB energy decreases in compressive loading at the yield point with respect to the undeformed configuration, in contrast to tensile loading.

1. Introduction

Much insight has been provided into the inelastic deformation behavior of nanocrystalline (NC) materials following the landmark paper by Gleiter [1]. Experiments showed that artifact-free bulk NC materials with a narrow grain size (< 100 nm) distribution exhibit tensile yield strength several times higher than that of their coarse-grained (CG) counterparts [2]. Unlike CG metals which are considered "yield" when a large number of dislocations are simultaneously transmitted across the grain boundaries (GBs) [3,4], the strength of an NC metal is mainly controlled by dislocation nucleation from GBs as a result of its inability to accomondate long range dislocation pile-up in individual grains. Indeed, GBs are especially important in NC metals due to the latter's high GB area to material volume ratio. In the last three decades, numerous experimental studies [5,6], continuum-based modeling [7], and atomisitc simulations [8,9] have been devoted to exploring plastically deformed NC metals, pointing to the need to understand the role played by dislocation nucleation from GBs in governing mechanical properties of NC materials [10].

As an NC metal contains a large number of GBs of different types and complex triple junctions, direct simulations of the NC metals are not desirable if one were to focus on responses of individual GBs. To isolate a GB from other lattice defects, the idealized sample containing only one GB, i.e., a bicrystal, is frequently used in experiments [11], multiscale modeling [12], and atomistic simulations [13]. It is found that besides the five macroscopic degrees of freedom (DOFs) that dictate a GB at the macroscopic level, atomic-level parameters such as the three microscopic DOFs, inter-atom deletion, local lattice rotation, GB ledges, interfacial porosity, and free volume spatial distribution may also significantly influence GB structures and corresponding dislocation nucleation [14]. When a Cu bicrystal is subject to a tensile loading, the natural conformation of the interface porosity with respect to the primary dislocation slip systems is responsible for the easy emission of Shockley partial dislocations from GBs containing a certain structural unit (SU) [15]. Of note is that most atomistic simulations of bicrystals so far considered face-centered cubic systems [16,17], while body-centered cubic (BCC) lattices which have more complicated plastic deformation mechanisms [18–21] are much less explored. On the other hand, investigations of dislocation nucleation from GBs in BCC systems are necessitated by the need to understand the plasticity of relevant NC materials.

Therefore, in this work, we utilize molecular dynamics (MD) simulations to investigate dislocation nucleation from six $\langle 112 \rangle$ symmetric tilt GBs subject to compressive loading along the GB plane normal direction. BCC vanadium (V) is chosen as the model material because V alloys are among the primary candidate first wall structural materials in fusion reactors [22] yet few prior MD simulations were devoted to the GBs in V or V alloys. Six single crystalline counterparts are also examined for reference. The remainder of the paper is organized as follows. It starts in Section 2 which details the process to create desired atomistic bicrys-

* Corresponding author.
E-mail address: shuozhixu@ucsb.edu (S. Xu).

https://doi.org/10.1016/j.physleta.2018.03.002
0375-9601/

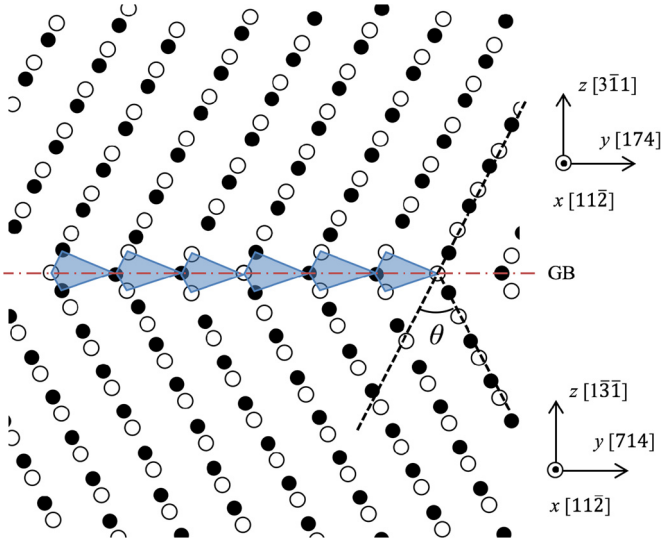

Fig. 1. A schematic of a bicrystal model with $\Sigma 11(1\bar{3}\bar{1})$ symmetric tilt GB, where the B SUs are highlighted in blue. Atoms on adjacent $(11\bar{2})$ planes are black and white, respectively. The misorientation angle θ is 62.96° in this case but needs to be varied for other GBs. (For interpretation of the colors in the figure(s), the reader is referred to the web version of this article.)

tal models. Then, in Section 3, the impacts of misorientation angle on slip system, yield stress, and GB energy are analyzed. Main findings are summarized in Section 4.

2. Methodology

A schematic of a bicrystal model is shown in Fig. 1, with the two grains rotated with respect to each other by a misorientation angle θ around a common $x[11\bar{2}]$ axis. The transformation matrix between the two crystallographic orientation systems can be written as a function of θ which is assumed positive for counterclockwise rotation, i.e.,

$$\begin{bmatrix} 1 & 0 & 0 \\ 0 & \cos\frac{\theta}{2} & \sin\frac{\theta}{2} \\ 0 & -\sin\frac{\theta}{2} & \cos\frac{\theta}{2} \end{bmatrix}$$

where θ varies from 34.04°, 62.96°, 85.14°, 101.54°, 122.88°, to 135.58° to produce six coincident site lattice (CSL) GBs with relatively low Σ, as listed in Table 1. Periodic boundary conditions are applied on all three axes, which effectively results in two identical, parallel, infinitely large GBs in one supercell [23]. The edge lengths of the simulation cell along each direction are set such that $L_x = 158.69$ Å, while L_y and L_z equal 32 times the corresponding lattice periodicity length. Since the atomistic simulation results significantly rely on the interatomic potential [24,25], two semi-empirical potentials — a modified embedded atom method (MEAM) potential [26] and a Finnis–Sinclair (FS) type potential [27] — are adopted for interactions between V atoms in a BCC lattice, with a lattice constant a_0 of 3.03686 Å and 3.03 Å, respectively.

As mentioned earlier, altering the five macroscopic DOFs that determine the CSL designation and GB plane does not result in unique GB structures [28]. To achieve the most probable equilibrium GB structures as in experiments, for each θ, 100 initial configurations considering a variety of in-plane (i.e., the x–y plane) rigid body translations and atom deletion criteria are created. For each configuration, energy minimization using a conjugate gradient algorithm is conducted [29,30], and the GB energy E_{GB} is calculated by

$$E_{GB} = \frac{E_{tot} - NE_{coh}}{2A_{GB}} \tag{1}$$

where E_{tot} is the total potential energy, N is the total number of atoms given in the last column of Table 1, $A_{GB} = L_x L_y$ is the GB area in one supercell, and E_{coh}, the cohesive energy of a V atom in a perfect lattice, is −5.3 eV for both potentials. It follows that, for each θ, the GB with the lowest E_{GB} among all 100 configurations is considered the equilibrium one [31] and is subject to homogeneous compressive loading in the plane stress condition along the z axis at a constant strain rate 10^9 s^{-1}. An NPT ensemble is adopted to maintain the temperature at 10 K and to zero the stress tensor components associated with the x and y directions. We remark that tensile simulation results of Cu bicrystals attained by high strain rates dynamic deformation at 10 K are similar to those by molecular statics at 0 K [13]; hence, the temperature we use is sufficiently low such that the thermal and mechanical effects do not intertwin. Compressive loading of six single crystals with the same crystal orientations as the lower grain in each case is also conducted for reference. All atomistic simulations are performed using LAMMPS [32] and atomic configurations are visualized in OVITO [33] with the lattice defects identified by the centrosymmetry parameter (CSP) [34].

3. Results and discussion

In all models, homogeneous dislocations are nucleated within the single crystals while dislocations are nucleated from GBs in the bicrystals. All dislocations are on {110} planes, with $(a_0/2)\langle 111\rangle$ Burgers vector. Snapshots of dislocation nucleation from $\Sigma 11(1\bar{3}\bar{1})$ and $\Sigma 35(\bar{1}\bar{5}\bar{3})$ GBs based on the MEAM potential [26] are shown in Fig. 2, while the FS potential [27] predicts the same activated slip systems. We also calculate the Schmid factor (SF) and the normal factor (NF) for the activated slip systems because they both have a significant effect on the dislocation nucleation from GBs [14,35,36]; specifically,

$$\mathrm{SF} = \cos\phi\cos\lambda \tag{2}$$

$$\mathrm{NF} = \cos\phi\sin\lambda \tag{3}$$

where ϕ is the angle formed between the loading axis (i.e., the z axis) and the slip plane normal direction, and λ is the angle be-

Table 1
The misorientation angle θ, CSL designation Σ, GB plane normal in terms of lower grain in Fig. 1, simulation cell size, and number of atoms for the six bicrystals.

Misorientation angle θ (°)	CSL designation and GB plane normal	Simulation cell size (Å)			Number of atoms
		L_x	L_y	L_z	
34.04	$\Sigma 35(3\bar{5}\bar{1})$	158.69	160.95	147.84	258462
62.96	$\Sigma 11(1\bar{3}\bar{1})$	158.69	143.54	146.50	227779
85.14	$\Sigma 59(1\bar{7}\bar{3})$	158.69	134.29	139.17	202356
101.54	$\Sigma 5(0\bar{2}\bar{1})$	158.69	141.94	130.38	201402
122.88	$\Sigma 35(\bar{1}\bar{5}\bar{3})$	158.69	147.53	147.84	236278
135.58	$\Sigma 7(\bar{1}\bar{3}\bar{2})$	158.69	148.44	155.83	251509

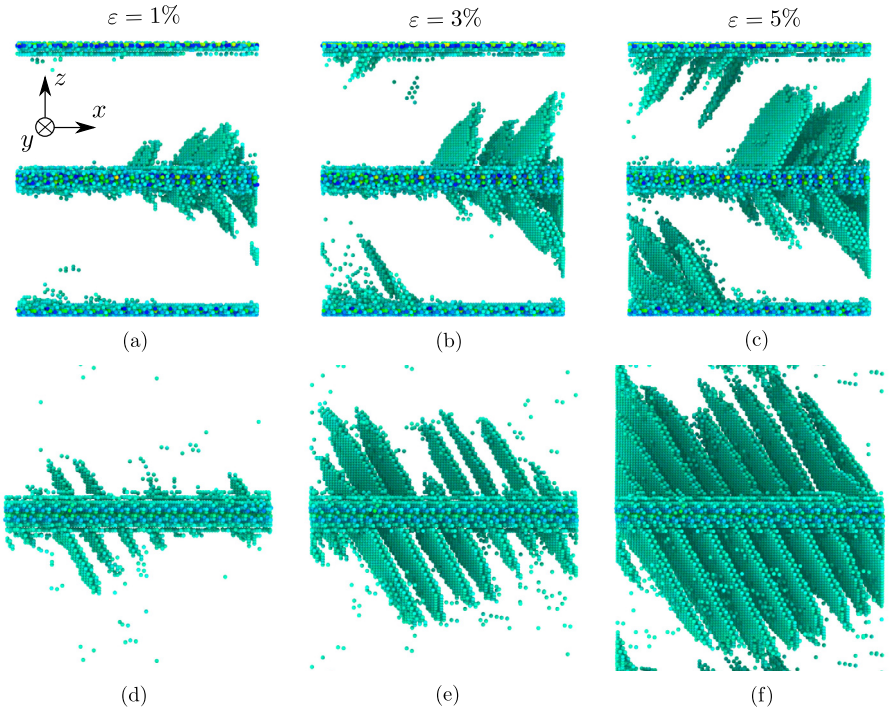

Fig. 2. Snapshots from MD simulations of bicrystals containing (a–c) $\Sigma 11(1\bar{3}\bar{1})$ GB and (d–f) $\Sigma 35(\bar{1}\bar{5}\bar{3})$ GB subject to compressive loading. Atoms are colored by CSP [34]; those with a CSP smaller than 1 are removed. Results are based on the MEAM potential [26] while those obtained using the FS potential [27] have the same activated slip systems.

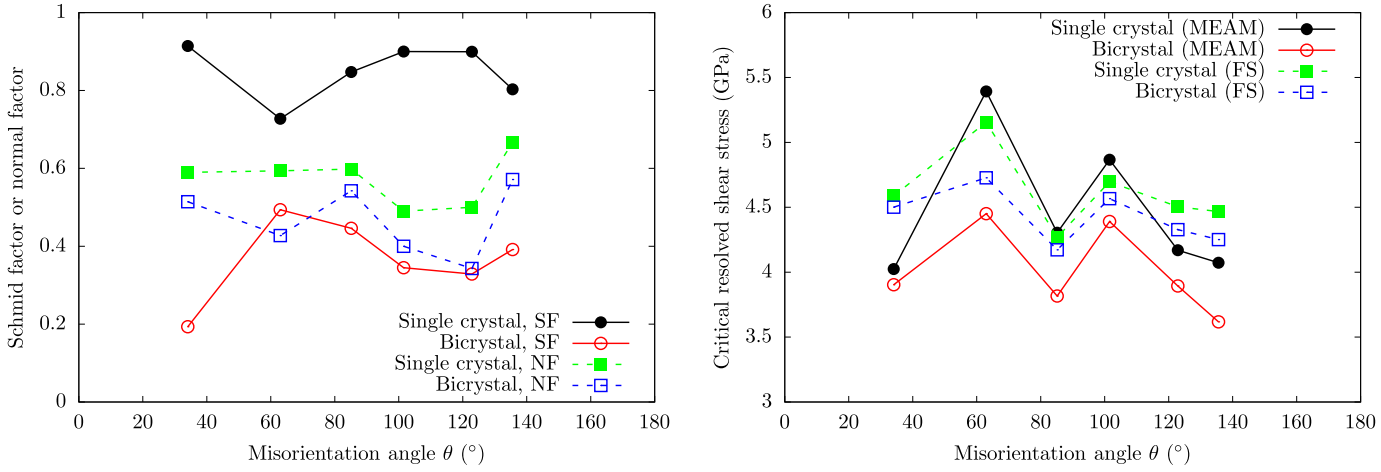

Fig. 3. Variation of (a) SF and NF, as well as (b) CRSS with the GB misorientation angle θ.

tween the loading axis and the slip direction. In all cases, both interatomic potentials predict that (i) except the two bicrystals with $\Sigma 5(0\bar{2}\bar{1})$ GB and $\Sigma 35(\bar{1}\bar{5}\bar{3})$ GB, the activated slip systems are not the one with the maximum SF, and (ii) the SF is higher than the NF, as plotted in Fig. 3(a). An analysis of the atomistic structures reveals that periodic embryonic dislocations on slip planes with the maximum SF are formed at the two peculiar GBs after energy minimization, i.e., prior to loading. Subsequently, these embryonic dislocations are emitted into the grain interior along their original slip planes under compressive loading. We remark that no energy minimized embryonic dislocations are observed in the other four GBs, nor in the single crystals.

With the help of SF, the critical resolved shear stress (CRSS) on the threshold of dislocation nucleation homogeneously in single crystals, τ_c^{si}, and that from GBs in bicrystals, τ_c^{bi}, as shown in Fig. 3(b), as well as the generalized ability of GBs to nucleate dislocations $(1 - \tau_c^{bi}/\tau_c^{si})$ following Ref. [23], as shown in Fig. 4(a). For all θ, both interatomic potentials predict that a smaller CRSS is required to nucleate dislocations in bicrystals than in single crystals, due to the absence of pre-existing lattice defects, i.e., GBs, in the latter, though different GBs have different generalized ability to nucleate dislocations.

Then, the GB energy E_{GB} for the undeformed bicrystals and for the configurations on the threshold of plasticity, i.e., dislocation initiation, are calculated following Eq. (1) with E_{coh} being the energy of a V atom in the correspondingly strained state in a perfect lattice. We remark that the calculated E_{GB} is of the same order of those ⟨112⟩-oriented symmetric tilt GBs in other BCC metals such as Fe, Mo, and Ta [37]. In our work, both potentials predict that the two peculiar GBs at which embryonic dislocations are formed after

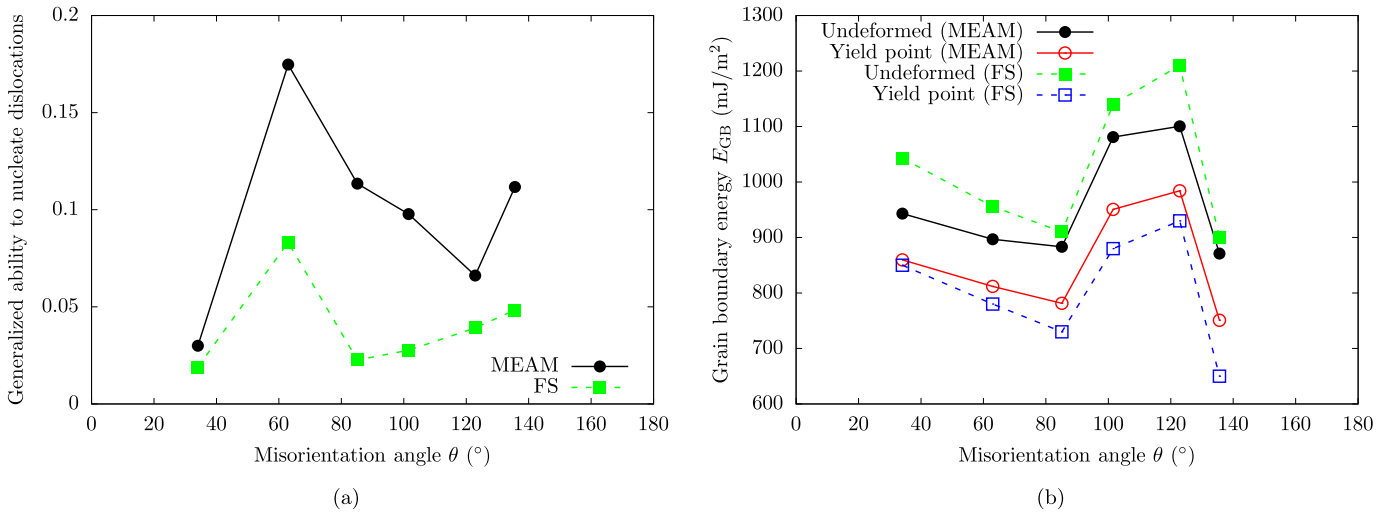

Fig. 4. Variation of (a) the generalized ability of GBs to nucleate dislocations and (b) GB energy E_{GB} with the GB misorientation angle θ.

energy minimization have the highest E_{GB}. For each GB, E_{GB} decreases at the yield point with respect to that for its undeformed configuration, as plotted in Fig. 4(b), in contrast to the tensile loading which increases E_{GB} on the threshold of plasticity [38]. A closer look at the GB structure reveals that the compressive loading suppresses the GB porosity, turning the local environment of GB atoms to that in a perfect lattice and thus lowering the GB energy. This justification agrees with the finding that for each GB, the reduction of E_{GB} during the elastic stage is more pronounced using the FS potential [27], which predicts an unrelaxed vacancy formation energy of 2.85 eV, than the MEAM potential [26], for which the same energy is 2.3 eV.

4. Conclusions

In this work, MD simulations are performed using two interatomic potentials to study dislocation nucleation from six symmetric tilt GBs in BCC V. Focus is on the impacts of the misorientation angle on activated slip systems, Schmid factor, normal factor, CRSS, and GB energy. Single crystals with the same crystallographic orientations as those of the lower grain in bicrystals are also investigated for reference. Results are summarized as follows:

1. Dislocations nucleate homogeneously in single crystals while from GBs in bicrystals; all dislocations are on {110} slip planes with $(a_0/2)\langle 111\rangle$ Burgers vector;
2. Breakdown of the Schmid law in BCC systems is observed for all six single crystals and four bicrystals; CRSS calculated with the help of the Schmid factor is found to be lower in bicrystals than in single crystals for the same misorientation angle;
3. The GB energy decreases with increasing compressive strain, in contrast to tensile loading which increases the GB energy.

While studying individual GBs is a necessary step toward a full grasp of NC metals, we emphasize that a collective knowledge of all GBs may not be directly employed to predict behavior of NC materials which may contain voids [39–41] and dislocation loops; in the future, we will employ more realistic simulation cells to better mimic the experiments and inform continuum models.

Acknowledgements

SX was supported in part by the Elings Prize Fellowship in Science offered by the California NanoSystems Institute (CNSI) on the UC Santa Barbara campus. SX also acknowledges support from the Center for Scientific Computing from the CNSI, MRL: an NSF MRSEC (DMR-1121053). This work used the Extreme Science and Engineering Discovery Environment (XSEDE), which is supported by National Science Foundation grant number ACI-1053575.

References

[1] H. Gleiter, Prog. Mater. Sci. 33 (1989) 223–315.
[2] K.M. Youssef, R.O. Scattergood, K.L. Murty, J.A. Horton, C.C. Koch, Appl. Phys. Lett. 87 (2005) 091904.
[3] S. Xu, L. Xiong, Y. Chen, D.L. McDowell, npj Comput. Mater. 2 (2016) 15016.
[4] S. Xu, L. Xiong, Y. Chen, D.L. McDowell, JOM 69 (2017) 814–821.
[5] G.J. Fan, L.F. Fu, H. Choo, P.K. Liaw, N.D. Browning, Acta Mater. 54 (2006) 4781–4792.
[6] L. Wang, P. Guan, J. Teng, P. Liu, D. Chen, W. Xie, D. Kong, S. Zhang, T. Zhu, Z. Zhang, E. Ma, M. Chen, X. Han, Nat. Commun. 8 (2017) 2142.
[7] J.Q. Zhou, R.T. Zhu, Z.Z. Zhang, Mater. Sci. Eng. A 480 (2008) 419–427.
[8] A. Hasnaoui, H. Van Swygenhoven, P.M. Derlet, Phys. Rev. B 66 (2002) 184112.
[9] P. Keblinski, D. Wolf, S.R. Phillpot, H. Gleiter, Scr. Mater. 41 (1999) 631–636.
[10] T.G. Langdon, Rev. Adv. Mater. Sci. 13 (2006) 6–14.
[11] M. Wojdyr, S. Khalil, Y. Liu, I. Szlufarska, Model. Simul. Mater. Sci. Eng. 18 (2010) 075009.
[12] F. Sansoz, J.F. Molinari, Acta Mater. 53 (2005) 1931–1944.
[13] M.A. Tschopp, G.J. Tucker, D.L. McDowell, Comput. Mater. Sci. 44 (2008) 351–362.
[14] D.E. Spearot, M.A. Tschopp, K.I. Jacob, D.L. McDowell, Acta Mater. 55 (2007) 705–714.
[15] M.A. Tschopp, G.J. Tucker, D.L. McDowell, Acta Mater. 55 (2007) 3959–3969.
[16] D. Chen, Y. Kulkarni, J. Appl. Mech. 82 (2015) 021005.
[17] D. Chen, Y. Kulkarni, J. Mech. Phys. Solids 84 (2015) 59–71.
[18] S.Z. Xu, Z.M. Hao, Y.Q. Su, Y. Yu, Q. Wan, W.J. Hu, Comput. Mater. Sci. 50 (2011) 2411–2421.
[19] S.Z. Xu, Z.M. Hao, Y.Q. Su, W.J. Hu, Y. Yu, Q. Wan, Radiat. Eff. Defects Solids 167 (2012) 12–25.
[20] S. Xu, Y. Su, Model. Simul. Mater. Sci. Eng. 24 (2016) 085015.
[21] S. Xu, J.K. Startt, T.G. Payne, C.S. Deo, D.L. McDowell, J. Appl. Phys. 121 (2017) 175101.
[22] D.M. Duffy, Philos. Trans. R. Soc. A 368 (2010) 3315–3328.
[23] T. Shimokawa, Phys. Rev. B 82 (2010) 174122.
[24] S.Z. Chavoshi, S. Xu, S. Goel, Proc. R. Soc. A 473 (2017) 20170084.
[25] S. Xu, Y. Su, S.Z. Chavoshi, Mater. Res. Express 5 (2018) 016523.
[26] M.I. Baskes, Phys. Rev. B 46 (1992) 2727–2742.
[27] S. Han, L.A. Zepeda-Ruiz, G.J. Ackland, R. Car, D.J. Srolovitz, J. Appl. Phys. 93 (2003) 3328–3335.
[28] S. Xu, Y. Su, D. Chen, L. Li, Appl. Phys. A 123 (2017) 788.
[29] S. Xu, S.Z. Chavoshi, Curr. Appl. Phys. 18 (2018) 114–121.
[30] S. Xu, S.Z. Chavoshi, Y. Su, Phys. Status Solidi RRL 12 (2018) 1700399.
[31] J.D. Rittner, D.N. Seidman, Phys. Rev. B 54 (1996) 6999–7015.
[32] S. Plimpton, J. Comput. Phys. 117 (1995) 1–19.
[33] A. Stukowski, Model. Simul. Mater. Sci. Eng. 18 (2010) 015012.
[34] C.L. Kelchner, S.J. Plimpton, J.C. Hamilton, Phys. Rev. B 58 (1998) 11085–11088.
[35] K. Kinoshita, T. Shimokawa, T. Kinari, Mater. Trans. 53 (2012) 147–155.
[36] R.D. Wyman, D.T. Fullwood, R.H. Wagoner, E.R. Homer, Acta Mater. 124 (2017) 588–597.

[37] E.N. Hahn, S.J. Fensin, T.C. Germann, M.A. Meyers, Scr. Mater. 116 (2016) 108–111.
[38] D.M. Saylor, A. Morawiec, G.S. Rohrer, Acta Mater. 51 (2003) 3675–3686.
[39] S.Z. Xu, Z.M. Hao, Q. Wan, IOP Conf. Ser., Mater. Sci. Eng. 10 (2010) 012175.
[40] Y. Su, S. Xu, Mater. Sci. Eng. A 678 (2016) 153–164.
[41] S. Xu, Y. Su, D. Chen, L. Li, Mater. Lett. 193 (2017) 283–287.